Topological nodal line semimetal with large nodal ring in an all-sp^2 hybridized carbon network formed by all-ten-membered carbon rings

Kun Bu[1,*] and Jian-Tao Wang[2,3,4,†]

[1]*School of Physics and Optoelectronic Engineering, Shandong University of Technology, Zibo 255000, China*

[2]*Beijing National Laboratory for Condensed Matter Physics, Institute of Physics, Chinese Academy of Sciences, Beijing 100190, China*

[3]*School of Physical Sciences, University of Chinese Academy of Sciences, Beijing 100049, China*

[4]*Songshan Lake Materials Laboratory, Dongguan, Guangdong 523808, China*

(Received 13 April 2023; revised 22 May 2023; accepted 31 May 2023; published 7 June 2023)

Carbon can form versatile allotropes due to its multiple bonding connections and the prediction of new carbon structures and properties has long been a hot topic. In 1983, Hoffmann *et al.* [J. Am. Chem. Soc. **105**, 4831 (1983)] have reported an all-sp^2 hybridized carbon allotrope with a 16-atom body-centered-tetragonal unit cell in $I4_1/amd$ (D_{4h}^{19}) symmetry, which is dubbed as cT16 carbon in this work. Here we report by *ab initio* calculations a systematical study on the structural, energetic, dynamical, and electronic properties of cT16 carbon. Interestingly, cT16 carbon is linked with *all-ten-membered* carbon rings. The phonon band spectrum calculations confirm its dynamical stability and *ab initio* molecular dynamics simulations prove its thermal stability up to 900 K. Previously cT16 carbon was widely considered as a simple metallic carbon. However, our detailed electronic band structures calculations reveal that cT16 is actually a *topological nodal line semimetal* with *a large closed nodal ring* centering the high-symmetric Γ point. It nearly encloses the entire $k_z = 0$ mirror plane, thus the drumheadlike surface bands can nearly cover the entire projected $(11\bar{1})$ surface Brillouin zone, which makes cT16 carbon an ideal nodal line semimetal. The simulated x-ray diffraction pattern of cT16 carbon matches well with one of the previously unexplained experimental peaks found in the diamond rich coatings grown on the stainless steel substrate. Our findings have provided insight for this well-known cT16 carbon, enriched the family of carbon allotropes with exotic topological electronic properties, suggested a viable route for its synthesis, and also provided an reasonable explanation for previous experimental data.

DOI: 10.1103/PhysRevB.107.245111

I. INTRODUCTION

Carbon can form diverse allotropes due to its ability to form sp, sp^2, and sp^3 hybridized carbon-carbon bonds [1]. Searching for new carbon allotropes with multiple experimental and theoretical techniques has long been an important subject in condensed matter physics and materials science. The zero-dimensional (0D) fullerene (C_{60}) [2], one-dimensional (1D) carbon nanotube [3], and two-dimensional (2D) graphene [4] are the most classical examples of the experimentally synthesized carbon allotropes. Very recently the two-dimensional and three-dimensioanl (3D) fullerene networks have been synthesized in multiple forms [5,6], which stir the interests of discovering more possible carbon phases. In recent years a series of carbon allotropes have also been proposed via *ab initio* calculations [7–12] and many of them have been included in the international database SACADA [13,14], and a highly efficient structural search method for carbon allotropes based on the labeled quotient graph has been developed [15,16]. An intriguing class of carbon phases are carbon allotropes with all-n-membered rings ($n \in \mathbb{Z}$), such as the all-sp^3 hybridized diamond, and previously proposed diamondlike carbon BC8 [17], BC12 [18], R16 [19], and O16 [20] with *all-six-membered* rings; all-sp^3 hybridized pentadiamond BC14 [21] and all-sp^2 hybridized pentagraphite mpg-C_8 [22] with *all-five-membered* rings.

Topological materials, including topological insulators (TIs) [23], topological superconductors (TSCs) [24,25], and topological semimetals (TSMs) [26] have been attracting tremendous research interests due to their protected boundary states and prospects for the future applications in quantum devices. The topological quantum chemistry [27] and symmetry-based indicator theory [28–31] have been established for the fast diagnosis of topological materials. The study of topological materials start from the gapped TIs and TSCs, and then extend to the gapless TSMs. The typical TSMs include the Weyl semimetals with twofold degenerate Weyl points coming in pairs [32–34], and Dirac semimetals with fourfold degenerate Dirac points [35–37], and nodal line semimetals with continuous line of band crossing nodes inside the first Brillouin zone (BZ) [38–43]. Among the three basic types, topological nodal line semimetals featuring the nearly flat topologically nontrivial surface states inside or outside the projected nodal lines, are often the precursors of other topological phases with proper added terms in the Hamiltonian [42]. Beyond the three fundamental types of TSMs, a series of emergent "new fermions" have been discovered in solids [44–49] and an "encyclopedia" of the emergent fermions have also been proposed [49].

*bukun94@163.com

†wjt@aphy.iphy.ac.cn

All-carbon based systems also host very rich topological phenomena. For example, the 2D graphene is a well-known Dirac semimetal [50], and a series of 3D carbon allotropes are proposed to be topological nodal line semimetals [51–66]. The fundamental types of topological nodal lines in all-carbon networks include A-type with closed nodal rings, such as in all-sp^2 hybridized MTC [52], bco-C_{16} [53], and bct-C_{16} carbon [54]; and B-type with two separate nodal lines such as in sp^2-sp^3 hybridized ign-C_6 [55], so-C_{12} [57], and oC24 carbon [56]. Some carbon allotropes with topological nodal lines are also revealed to hold good transport properties, for example the HZGM-42 carbon [61] is proposed to be a promising anode material for lithium-ion batteries and oC46 carbon [62] for sodium-ion batteries. The study for the topological physics in all-carbon materials never ceases and many new topological states have been proposed in all-carbon based materials, including unconventional nodal line configurations such as nodal net in bct-C_{40} carbon [66], hybrid nodal chain in oP-C_{24} carbon [65]; higher-order topological states such as second- order topological insulator in 2D graphdiyne [67,68], and second-order real nodal line semimetals in 3D graphdiyne [69]. Also, topological flat band and fragile topology [70–75] in "magic angle" twisted bilayer graphene [76–79], which indicates that carbon is a playground for the exploration of topological physics and more topological states are yet to be discovered.

In 1983, an all-sp^2 hybridized carbon allotrope with a 16-atom body-centered tetragonal unit cell in $I4_1/amd$ (D_{4h}^{19}) symmetry (space group No. 141), which is dubbed as cT16 carbon in the present paper was proposed by Hoffmann *et al.* [80]. In this work, we perform a systematical study on the structural, energetic, dynamical, and electronic properties on this carbon phase with *ab initio* calculations. Interestingly, the carbon atoms in cT16 carbon form *all-ten-membered* carbon rings. The dynamical stability of cT16 carbon has been confirmed with phonon band spectrum calculations and the thermal stability of cT16 carbon up to 900 K has been confirmed with *ab initio* molecular dynamics simulations. Previously cT16 carbon was widely thought to be a simple metallic carbon phase [80], however, our detailed band structure calculations show that cT16 carbon is actually a *topological nodal line semimetal* with a closed A-type nodal ring centering the high-symmetric Γ point protected by the spatial inversion ($\mathcal{P}$) and time reversal ($\mathcal{T}$) symmetries, and restricted onto the $k_z = 0$ mirror plane due to the $\mathcal{M}_z$ mirror symmetry. Although the proposals for carbon allotropes with A-type nodal rings are already comprehensive, the nodal ring in cT16 carbon encloses nearly the entire $k_z = 0$ mirror plane, which is the *largest nodal ring* among the yet reported carbon phases with A-type nodal rings [52–54,59,64]. Thus, the projected surface BZ is nearly covered entirely by the nearly flat topologically nontrivial surface states, manifesting that cT16 carbon is an ideal platform for the study of flat band physics, superconductivity and electronic correlations [81,82]. The simulated x-ray diffraction (XRD) pattern of cT16 carbon matches well with one of the experimental peaks found in the diamond rich coatings grown on the stainless substrate [83], while the peak is unexplained in previous theoretical proposals [20,64]. Our findings have provided insights for the physical properties of this well-known carbon allotrope, provided an reasonable explanation for the previously unexplained experimental data, and shed light on the possible synthesis root for cT16 carbon.

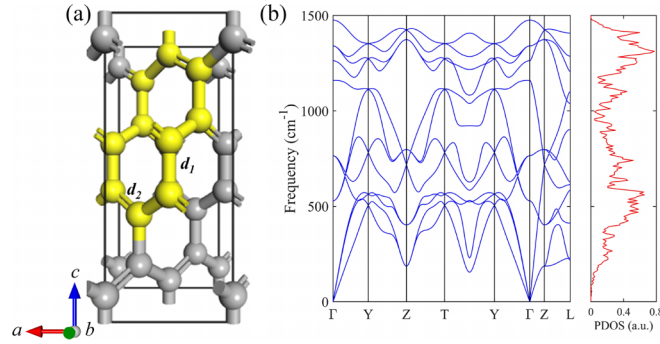

FIG. 1. (a) The unit cell of cT16 carbon with lattice parameters $a = b = 3.5468$ Å and $c = 8.5829$ Å. There is only one kind of carbon atoms occupying the 16*h* (0.0, 0.0, 0.9142) Wyckoff position. There are two kinds of bond lengths of $d_1 = 1.472$ Å and $d_2 = 1.423$ Å. (b) The phonon band spectrum and phonon density of states (PDOS) for cT16 carbon. There is no imaginary frequency in the entire BZ and PDOS.

II. COMPUTATIONAL METHOD

Our *ab initio* calculations are performed with the Vienna *ab initio* simulation package (VASP). The generalized gradient approximation (GGA) [84] developed by Armiento-Mattsson (AM05) [85] is used as the exchange-correlation potential. The all-electron projector augmented wave [86] method is used and the $2s^2 2p^2$ electrons are treated as valence electrons. We use a plane-wave basis set with an energy cutoff of 800 eV. The BZ is sampled with a $8 \times 8 \times 8$ Monkhorst-Pack $\boldsymbol{k}$-point grid. The geometries are optimized with symmetry constraints until the remaining atomic forces are less than 10^{-3} eV/Å and the energy convergence criterion is set to 10^{-6} eV. Electronic band structures are calculated using the GGA-Perdue-Burke-Ernzerhof method [87] and checked with the Heyd-Scuseria-Ernzerhof hybrid functional [88] method. Phonon band structures and force constants calculations are performed using the phonopy package [89] with the finite displacement method. To further explore the topological electronic properties of this carbon allotrope, we have built tight-binding (TB) models with the maximally localized Wannier functions (MLWFs) implemented in the Wannier90 package [90,91]. Based on the constructed TB models, we have calculated topological invariants and the topological surface states using the WannierTools package [92].

III. RESULTS AND DISCUSSIONS

We firstly present the crystalline structures of cT16 carbon. The unit cell of cT16 carbon is presented in Fig. 1(a). The cT16 carbon is in an all-sp^2 hybridized carbon network with 16 carbon atoms in $I4_1/amd$ (D_{4h}^{19}) symmetry (space group No. 141). The lattice parameters for cT16 carbon are $a = b = 3.5468$ Å, and $c = 8.5829$ Å. There is only one kind of carbon atom occupying the 16*h* (0.0, 0.0, 0.9142) Wyckoff position. There are two kinds of bond lengths of $d_1 = 1.472$ Å and

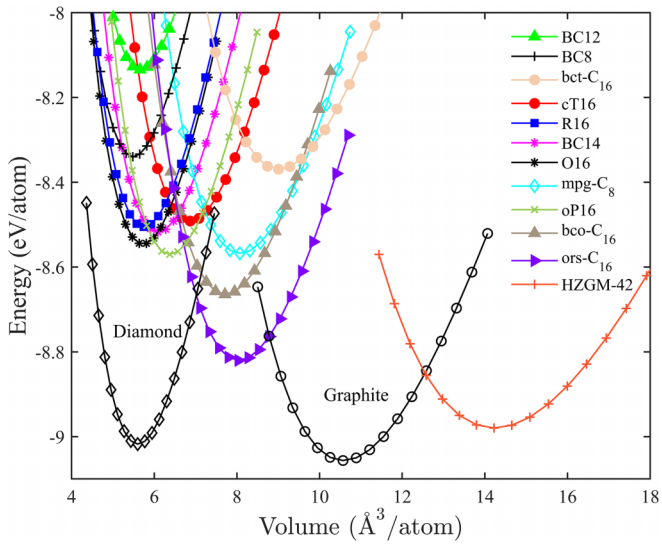

FIG. 2. The energy versus volume per atom for cT16 carbon, comparing with diamond, graphite, and the previously reported BC12 [18], BC8 [17], R16 [19], and O16 carbon [20] with all-six-membered carbon rings, BC14 [21] and mpg-C_8 carbon [22] with all-five-membered carbon rings, bct-C_{16} [54], oP16 [64], bco-C_{16} [53], ors-C_{16} [59], and HZGM-42 carbon [61] with topological nodal lines.

$d_2 = 1.423$ Å. Interestingly, cT16 carbon can be visualized as the interconnections of *all-ten-membered* carbon rings as colored in yellow in Fig. 1(a). Along with the diamondlike BC8 [17], BC12 [18], R16 [19] and O16 [20] carbon comprising of *all-six-membered* carbon rings; pentadiamond BC14 [21] and pentagraphite mpg-C_8 [22] comprising of *all-five-membered* carbon rings, these carbon allotropes with all-*n*-membered ($n \in \mathbb{Z}$) carbon rings form a rare family among the proposed carbon phases.

Figure 2 shows the calculated energy versus volume per atom for cT16 carbon, comparing with diamond, graphite, and previously reported BC12 [18], BC8 [17], R16 [19], and O16 carbon [20] with *all-six-membered* carbon rings; BC14 [21] and mpg-C_8 carbon [22] with *all-five-membered* carbon rings; bct-C_{16} [54], oP16 [64], bco-C_{16} [53], ors-C_{16} [59], and HZGM-42 carbon [61] with topological nodal lines. The equilibrium energy for cT16 carbon is about −8.49 eV/atom. The energy stability of the above carbon allotropes obeys the following sequence: BC12 < BC8 < bct-C_{16} < cT16 < R16 < BC14 < O16 < mpg-C_8 < oP16 < bco-C_{16} < ors-C_{16} < HZGM-42 < diamond < graphite. By fitting the energy versus volume curve using the Murnaghan equation of states [93], the bulk modulus B_0 for cT16 is calculated to be 216 GPa. We list the structural parameters (including the lattice parameters, volume, bond lengths, bulk modulus B_0, and calculated band gaps) for the above structures in Table I, along with the available experimental data for diamond [94].

To check the mechanical stability of cT16 carbon, we have calculated the elastic constants of cT16 carbon as $C_{11} =$ 451 GPa, $C_{33} = 1217$ GPa, $C_{44} = 363$ GPa, $C_{66} = 209$ GPa, $C_{12} = 410$ GPa, and $C_{13} = 75$ GPa, which satisfies the criteria of the mechanical stability for tetragonal phase [95] as $C_{11} > 0$, $C_{33} > 0$, $C_{44} > 0$, $C_{66} > 0$, $(C_{11} - C_{12}) > 0$, $(C_{11} + C_{33} - 2C_{13}) > 0$, $[2(C_{11} + C_{12}) + C_{33} + 4C_{13}] > 0$. To examine the dynamical stability of cT16 carbon, we have calculated the phonon band spectrum and phonon density of states (PDOS) as shown in Fig. 1(b). The highest phonon vibrational frequency is about 1500 cm^{-1} locating at the high-symmetric Γ point. There is no imaginary frequency in the entire BZ and PDOS, thus confirming the dynamical stability of cT16 carbon.

To confirm the thermal stability of cT16 carbon, we have performed *ab initio* molecular dynamics (AIMD) simulations using a 2 × 2 × 1 supercell with 64 carbon atoms. We have used the canonical (*NVT*) ensembles at the temperature of 300, 600, and 900 K by the Nosé thermostat [96] with the step of 1 fs. The energy fluctuations at 900 K are shown in Fig. 3, while the simulation results for 300 K and 600 K are given in Fig. S1 of the Supplemental Material [97]. After

TABLE I. Calculated equilibrium structural parameters (space group, lattice parameters a, b, and c, angle α, volume per atom V_0, bond lengths d_{C-C}), total energy E_{tot} per atom, electronic band gap E_g, and bulk modulus (B_0) for diamond, BC8 [17], BC12 [18], R16 [19], O16 [20], BC14 [21], mpg-C_8 [22], bct-C_{16} [54], oP16 [64], bco-C_{16} [53], ors-C_{16} [59], HZGM-42 [61], and cT16 carbon at zero pressure, compared to available experimental data [94].

Structure	Space group	Method	a (Å)	b (Å)	c (Å)	α (°)	V_0 (Å^3)	d_{C-C} (Å)	E_{tot} (eV)	E_g (eV)	B_0 (GPa)
Diamond	$Fd\bar{3}m$	AM05	3.552				5.60	1.538	−9.018	5.36	451
		Exp [94]	3.567				5.67	1.544		5.47	446
BC8	$Ia\bar{3}$	AM05 [18]	4.443				5.48	1.617	−8.340	3.58	407
BC12	$Ia\bar{3}d$	AM05 [18]	5.139		5.66		5.66	1.574	−8.134	2.98	429
R16	$R\bar{3}c$	AM05 [19]	4.514			90.88	5.75	1.466–1.755	−8.505	4.45	386
O16	$Pbcn$	AM05 [20]	4.405	4.740	4.384		5.64	1.493–1.730	−8.546	4.07	417
BC14	$I2_13$	AM05 [21]	5.545				6.09	1.498–1.824	−8.517	5.64	386
mpg-C_8	$C2/m$	AM05 [22]	6.389	7.053	3.299		8.07	1.364–1.493	−8.568	Semimetal	285
bct-C_{16}	$I4_1/amd$	AM05 [54]	6.592	6.592	3.377		9.17	1.362–1.438	−8.539	Semimetal	165
oP16	$Pcca$	AM05 [64]	4.646	4.277	5.133		6.37	1.353–1.691	−8.570	Semimetal	370
bco-C_{16}	$Imma$	AM05 [53]	7.806	4.877	3.237		7.70	1.382–1.459	−8.671	Semimetal	315
ors-C_{16}	$Cccm$	AM05 [59]	3.318	8.372	4.915		8.02	1.421–1.438	−8.810	Semimetal	298
HZGM-42	$P63/mcm$	AM05 [61]	16.750	16.750	2.458	120	14.22	1.413–1.520	−8.980	Semimetal	169
cT16	$I4_1/amd$	AM05	3.547	3.547	8.583		6.87	1.423–1.472	−8.492	Semimetal	216

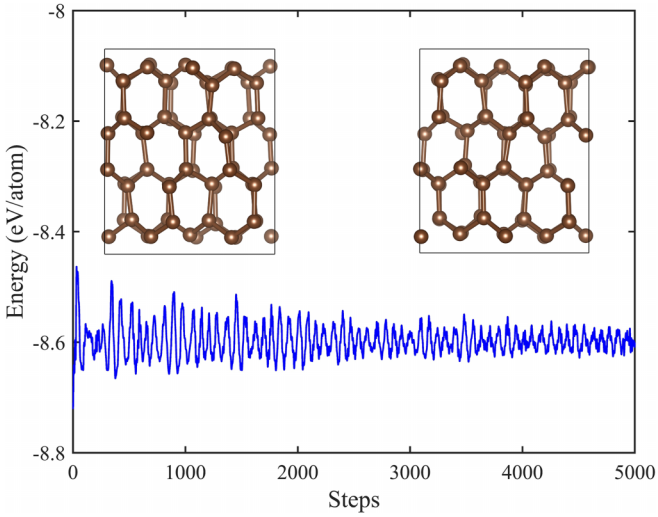

FIG. 3. The energy fluctuations of cT16 carbon during the AIMD simulations at the temperature of 900 K using a $2 \times 2 \times 1$ supercell. The inset structures show the crystalline structures at step 1000 and 4000.

heating up the system for 5 ps, there is no obvious structural change occurs. Some carbon atoms may slightly deviate from the initial equilibrium positions, but they are expected to go back to the initial equilibrium positions after proper structural relaxations, which indicates that cT16 is a stable carbon phase even at the high temperature of 900 K.

Next we discuss the electronic properties of cT16 carbon. Fig. 4(a) shows the calculated bulk band structures of cT16 carbon. It can be seen that there are some band crossing points around the Fermi level (E_F) along the high-symmetric Γ-T, T-Y, and Γ-Y directions due to the band inversion mechanism [23–26] with opposite parities and $\mathcal{M}_z$ mirror eigenvalues. Previously, cT16 was widely thought as a simple metallic carbon [80]. However, the detailed analysis of the band structures in the 3D BZ shows that cT16 carbon is a *topological nodal line semimetal* with an A-type closed nodal ring centering the high-symmetric Γ point in the $k_z = 0$ mirror plane, which is like the previously proposed MTC [52], bco-C_{16} [53], bct-C_{16} [54], oP16 [64], and ors-C_{16} carbon [59], as shown in Fig. 4(b). Notably, the nodal ring in cT16 carbon nearly encloses the entire $k_z = 0$ mirror plane, indicating that cT16 carbon holds the *largest close nodal ring* among the yet proposed carbon allotropes with A-type nodal rings.

The nodal ring in cT16 carbon is enforced due to the band inversion mechanism [23–26] and protected by $\mathcal{PT}$ symmetries, and restricted onto the $k_z = 0$ mirror plane due to the $\mathcal{M}_z$ symmetry. To further understand the topological origin of the nodal ring in cT16 carbon, we have calculated the symmetry-based indicators $\mathbb{Z}_{2,2,2,4} = (z_{2,1}, z_{2,2}, z_{2,3}, z_4)$ by counting the parities at the time reversal invariant momenta (TRIM) points for the occupied states, which can be expressed as [28–31]:

$$z_{2,i} = \sum_{\substack{\boldsymbol{K}\in\text{TRIM} \\ \text{at}\{k_i=\pi\}}} \frac{N_-(\boldsymbol{K}) - N_+(\boldsymbol{K})}{2} \mod 2,$$
$$z_4 = \sum_{\boldsymbol{K}\in\text{TRIM}} \frac{N_-(\boldsymbol{K}) - N_+(\boldsymbol{K})}{2} \mod 4. \quad (1)$$

$N_+(\boldsymbol{K})$ ($N_-(\boldsymbol{K})$) means the number of bands with even (odd) parities at the TRIM points, which are given in Table S1 in the Supplemental Material [97]. In this case, the symmetry-based indicators for cT16 are calculated to be $(z_{2,1}, z_{2,2}, z_{2,3}, z_4) = (0, 0, 0, 1)$. Then according to Ref. [30], there may be a nodal ring in the $k_i = 0$ ($i = x, y, z$) plane. Thus the nodal ring in the $k_z = 0$ mirror plane can be understood from the symmetry-based indicator perspective.

To further understand the electronic properties of cT16 carbon, we have calculated the orbital projected density of states for cT16 carbon as shown in Fig. S2(a) in the Supplemental Material [97]. Meanwhile, we have also performed a fat band analysis to show the orbital contributions for the band structures of cT16 carbon as shown in Fig. S2(b)–2(d) of the Supplemental Material [97]. The electronic states around the E_F are mainly contributed by the carbon p_x orbitals. Then we have built a four-band TB model based on the carbon p_x orbitals using the MLWFs as shown in Fig. S2(e) of the Supplemental Material [97]. It is well-know that, when the nodal line is projected onto a certain plane, there should be a drumheadlike topologically nontrivial surface state inside the nodal line [39,41,42,98]. Based on the established TB models, we have calculated the $(11\bar{1})$ surface states using the iterative Green's function method along the projected $\overline{\text{T}}$-$\overline{\Gamma}$-$\overline{\text{Y}}$ direction

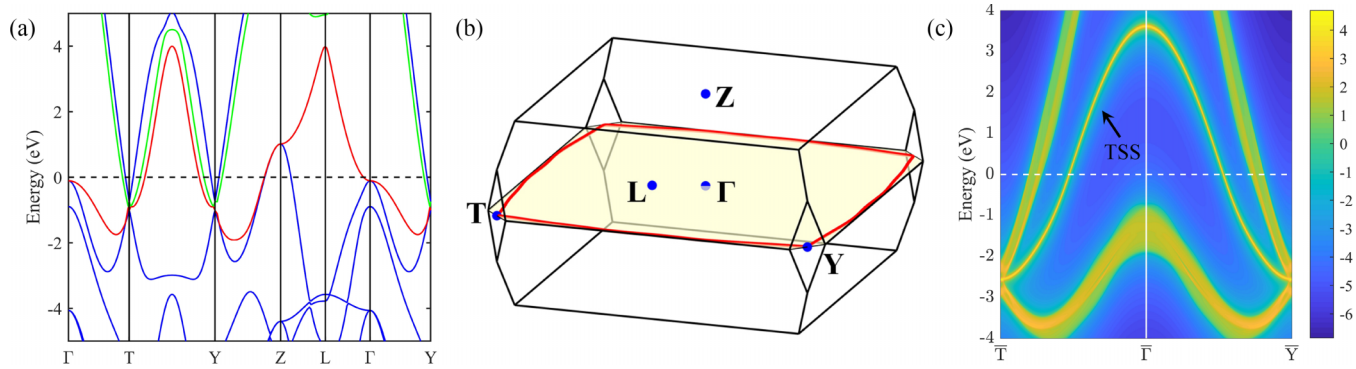

FIG. 4. (a) The bulk band structures of cT16 carbon. The Fermi level (E_F) is set to zero; (b) The first BZ and an A-type closed nodal ring of cT16 carbon, which is nearly enclosing the entire $k_z = 0$ mirror plane (shaded with yellow); (c) The $(11\bar{1})$ topological surface state (TSS) of cT16 carbon along the projected $\overline{\text{T}}$-$\overline{\Gamma}$-$\overline{\text{Y}}$ path.

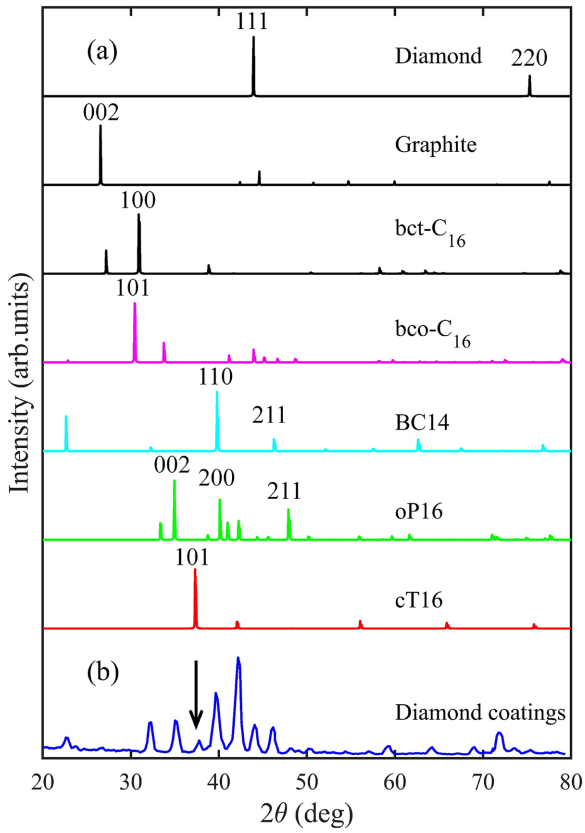

FIG. 5. (a) The simulated x-ray diffraction pattern (XRD) for cT16 carbon, comparing with diamond, graphite, bct-C_{16} [54], bco-C_{16} [54], BC14 [21], and oP16 carbon [64]; (b) The experimental data obtained from the diamond rich coatings on the stainless steel substrate [83]. The x-ray wavelength is 1.5406 Å with a copper source.

[Fig. 4(c)]. The surface states along the projected $\overline{\Gamma}$-$\overline{\Gamma}$ and $\overline{\Gamma}$-$\overline{\Upsilon}$ directions show similar dispersions due to the fourfold rotational symmetry of the $k_z = 0$ mirror plane, and can be seen inside the nodal ring connecting the two Dirac points and nearly covering the entire projected BZ, which can be detected using the angle resolved photoemission spectroscopy technique [99].

Finally, to make a connection with experiment, we have simulated the XRD pattern of cT16 carbon, along with diamond, graphite, and previously reported bct-C_{16} [54], bco-C_{16} [53], BC14 [21], and oP16 carbon [64], and compare with the experimental XRD data obtained from the diamond rich coatings grown on the stainless steel substrate [83], as shown in Fig. 5. The (101) peak of cT16 carbon around 37° matches with one of the experimental peaks, which is unexplained in the previous theoretical proposals [20,64], indicating that cT16 carbon may be one of the findings discovered in this experiment, and also provide an viable route for the synthesis of cT16 carbon.

IV. SUMMARY

In summary, based on *ab initio* calculations, we have performed systematic studies on the structural, energetic, dynamical, and electronic properties for the all-sp^2 hybridized cT16 carbon. Phonon spectrum calculations and *ab initio* molecular dynamics simulations show that cT16 is a dynamically and thermally stable carbon phase. Electronic band structure calculations show that cT16 is a topological nodal line semimetal holding *the largest nodal ring* among the reported topological carbon phases. The XRD pattern of cT16 carbon matches well with one of the experimental peaks found in the diamond rich coatings on the stainless steel substrate, indicating that cT16 may be one of the modifications found in the experiment. Our findings have provided new insights for the physical properties of this well-known cT16 carbon, identified a carbon allotrope with the largest nodal ring, and shed light on its possible synthesis route.

ACKNOWLEDGMENTS

K.B. acknowledges the helpful discussions with M. Zhang and Y. Wang. J.-T.W. acknowledges the support from the Strategic Priority Research Program of the Chinese Academy of Sciences (Grant No. XDB33000000), the National Natural Science Foundation of China (Grants No. 11674364, No. 11974387, and No. 92263202), and the National Key Research and Development Program of China (Grant No. 2020YFA0711502).

[1] A. T. Balaban, Carbon and its nets, Comput. Math. Appl. **17**, 397 (1989).
[2] H. W. Kroto, J. R. Heath, S. C. O'Brien, R. F. Curl, and R. E. Smalley, C_{60}: Buckminsterfullerene, Nature (London) **318**, 162 (1985).
[3] S. Iijima, Helical microtubules of graphitic carbon, Nature (London) **354**, 56 (1991).
[4] K. S. Novoselov, A. K. Geim, S. V. Morozov, D. Jiang, Y. Zhang, S. V. Dubonos, I. V. Grigorieva, and A. A. Firsov, Electric field effect in atomically thin carbon films, Science **306**, 666 (2004).
[5] L. Hou, X. Cui, B. Guan, S. Wang, R. Li, Y. Liu, D. Zhu, and J. Zheng, Synthesis of a monolayer fullerene network, Nature (London) **606**, 507 (2022).
[6] F. Pan, K. Ni, T. Xu, H. Chen, Y. Wang, K. Gong, C. Liu, X. Li, M. L. Lin, S. Li, X. Wang, W. Yan, W. Yin, P. H. Tan, L. Sun, D. Yu, R. S. Ruoff, and Y. Zhu, Long-range ordered porous carbons produced from C_{60}, Nature (London) **614**, 95 (2023).
[7] Q. Li, Y. Ma, A. R. Oganov, H. Wang, H. Wang, Y. Xu, T. Cui, H. K. Mao, and G. Zou, Superhard Monoclinic Polymorph of Carbon, Phys. Rev. Lett. **102**, 175506 (2009).
[8] K. Umemoto, M. R. Wentzcovitch, S. Saito, and T. Miyake, Body-Centered Tetragonal C_4: A Viable sp^3 Carbon Allotrope, Phys. Rev. Lett. **104**, 125504 (2010).
[9] J. T. Wang, C. F. Chen, and Y. Kawazoe, Low-Temperature Phase Transformation from Graphite to sp^3 Orthorhombic Carbon, Phys. Rev. Lett. **106**, 075501 (2011).

[10] M. Amsler, J. A. Flores-Livas, L. Lehtovaara, F. Balima, S. A. Ghasemi, D. Machon, S. Pailhès, A. Willand, D. Caliste, S. Botti, A. S. Miguel, S. Goedecker, and M. A. L. Marques, Crystal Structure of Cold Compressed Graphite, Phys. Rev. Lett. **108**, 065501 (2012).

[11] X. L. Sheng, Q. B. Yan, F. Ye, Q. R. Zheng, and G. Su, T-Carbon: A Novel Carbon Allotrope, Phys. Rev. Lett. **106**, 155703 (2011).

[12] J. T. Wang, C. F. Chen, and Y. Kawazoe, New cubic carbon phase via graphitic sheet rumpling, Phys. Rev. B **85**, 214104 (2012).

[13] D. M. Proserpio *et al.*, Samara Carbon Allotrope Database, http://sacada.sctms.ru.

[14] R. Hoffmann, A. A. Kabanov, A. A. Golov, and D. M. Proserpio, Homo citans and carbon allotropes: For an ethics of citation, Angew. Chem. Int. Ed. **55**, 10962 (2016).

[15] C. He, X. Shi, S. J. Clark, J. Li, C. J. Pickard, T. Ouyang, C. Zhang, C. Tang, and J. Zhong, Complex Low Energy Tetrahedral Polymorphs of Group IV Elements from First Principles, Phys. Rev. Lett. **121**, 175701 (2018).

[16] X. Shi, S. Li, J. Li, T. Ouyang, C. Zhang, C. Tang, C. He, and J. Zhong, High-Throughput Screening of Two-dimensional planar sp^2 carbon space associated with a labeled quotient graph, J. Phys. Chem. Lett. **12**, 11511 (2021).

[17] M. T. Yin, Si-III (BC-8) crystal phase of Si and C: Structural properties, phase stabilities, and phase transitions, Phys. Rev. B **30**, 1773 (1984).

[18] Z. Z. Li, C. S. Lian, J. Xu, L. F. Xu, J. T. Wang, and C. F. Chen, Computational prediction of body-centered cubic carbon in an all-sp^3 six-member ring configuration, Phys. Rev. B **91**, 214106 (2015).

[19] Z. Z. Li, J. T. Wang, H. Mizuseki, and C. F. Chen, Computational discovery of a new rhombohedral diamond phase, Phys. Rev. B **98**, 094107 (2018).

[20] K. Bu, J. T. Wang, Z. Z. Li, H. Mizuseki, and Y. Kawazoe, A superhard orthorhombic carbon with all six-membered-ring in sp^3 bonding networks, Phys. Lett. A **383**, 2809 (2019).

[21] J. T. Wang, C. F. Chen, and H. Mizuseki, Body centered cubic carbon BC14: An all-sp^3 bonded full-fledged pentadiamond, Phys. Rev. B **102**, 184106 (2020).

[22] J. T. Wang, K. Bu, Y. Qian, H. Weng, and C. F. Chen, Pentagraphite C_8: An all-$sp^2$2 topological nodal-line semimetal, Phys. Rev. B **104**, 245143 (2021).

[23] M. Z. Hasan and C. L. Kane, Colloquium: Topological insulators, Rev. Mod. Phys. **82**, 3045 (2010).

[24] X. L. Qi and S. C. Zhang, Topological insulators and superconductors, Rev. Mod. Phys. **83**, 1057 (2011).

[25] C. K. Chiu, J. C. Y. Teo, A. P. Schnyder, and S. Ryu, Classification of topological quantum matter with symmetries, Rev. Mod. Phys. **88**, 035005 (2016).

[26] N. P. Armitage, E. J. Mele, and A. Vishwanath, Weyl and Dirac semimetals in three-dimensional solids, Rev. Mod. Phys. **90**, 015001 (2018).

[27] B. Bradlyn, L. Elcoro, J. Cano, M. G. Vergniory, Z. Wang, C. Felser, I. M. Aroyo, and B. Andrei Bernevig, Topological quantum chemistry, Nature (London) **547**, 298 (2017).

[28] H. C. Po, A. Vishwanath, and H. Watanabe, Symmetry-based indicators of band topology in the 230 space groups, Nat. Commun. **8**, 50 (2017).

[29] Z. Song, T. Zhang, Z. Fang, and C. Fang, Quantitative mappings between symmetry and topology in solids, Nat. Commun. **9**, 3530 (2018).

[30] Z. Song, T. Zhang, and C. Fang, Diagnosis for Nonmagnetic Topological Semimetals in the Absence of Spin-Orbital Coupling, Phys. Rev. X **8**, 031069 (2018).

[31] J. Kruthoff, J. de Boer, J. van Wezel, C. L. Kane, and R. J. Slager, Topological Classification of Crystalline Insulators through Band Structure Combinatorics, Phys. Rev. X **7**, 041069 (2017).

[32] X. Wan, A. M. Turner, A. Vishwanath, and S. Y. Savrasov, Topological semimetal and Fermi-arc surface states in the electronic structure of pyrochlore iridates, Phys. Rev. B **83**, 205101 (2011).

[33] H. Weng, C. Fang, Z. Fang, B. Andrei. Bernevig, and X. Dai, Weyl Semimetal Phase in Noncentrosymmetric Transition-Metal Monophosphides, Phys. Rev. X **5**, 011029 (2015).

[34] G. Xu, H. Weng, Z. Wang, X. Dai, and Z. Fang, Chern Semimetal and the Quantized Anomalous Hall Effect in $HgCr_2Se_4$, Phys. Rev. Lett. **107**, 186806 (2011).

[35] Z. Wang, Y. Sun, X. Q. Chen, C. Franchini, G. Xu, H. Weng, X. Dai, and Z. Fang, Dirac semimetal and topological phase transitions in A_3Bi (A = Na, K, Rb), Phys. Rev. B **85**, 195320 (2012).

[36] Z. Wang, H. Weng, Q. Wu, X. Dai, and Z. Fang, Three-dimensional Dirac semimetal and quantum transport in Cd_3As_2, Phys. Rev. B **88**, 125427 (2013).

[37] Q. D. Gibson, L. M. Schoop, L. Muechler, L. S. Xie, M. Hirschberger, N. P. Ong, R. Car, and R. J. Cava, Three-dimensional Dirac semimetals: Design principles and predictions of new materials, Phys. Rev. B **91**, 205128 (2015).

[38] M. Phillips and V. Aji, Tunable line node semimetals, Phys. Rev. B **90**, 115111 (2014).

[39] Y. Kim, B. J. Wieder, C. L. Kane, and A. M. Rappe, Dirac Line Nodes in Inversion-Symmetric Crystals, Phys. Rev. Lett. **115**, 036806 (2015).

[40] R. Yu, H. Weng, Z. Fang, X. Dai, and X. Hu, Topological Node-Line Semimetal and Dirac Semimetal State in Antiperovskite Cu_3PdN, Phys. Rev. Lett. **115**, 036807 (2015).

[41] C. Fang, Y. Chen, H. Y. Kee, and L. Fu, Topological nodal line semimetals with and without spin-orbital coupling, Phys. Rev. B **92**, 081201(R) (2015).

[42] C. Fang, H. Weng, X. Dai, and Z. Fang, Topological nodal line semimetals, Chin. Phys. B **25**, 117106 (2016).

[43] Q. Xu, R. Yu, Z. Fang, X. Dai, and H. Weng, Topological nodal line semimetals in the CaP_3 family of materials, Phys. Rev. B **95**, 045136 (2017).

[44] B. Bradlyn, J. Cano, Z. Wang, M. G. Vergniory, C. Felser, R. J. Cava, and B. A. Bernevig, Beyond Dirac and Weyl fermions: Unconventional quasiparticles in conventional crystals, Science **353**, aaf5037 (2016).

[45] G. Chang, S. Y. Xu, B. J. Wieder, D. S. Sanchez, S. M. Huang, I. Belopolski, T. R. Chang, S. Zhang, A. Bansil, H. Lin, and M. Z. Hasan, Unconventional Chiral Fermions and Large Topological Fermi Arcs in RhSi, Phys. Rev. Lett. **119**, 206401 (2017).

[46] Z. Rao, H. Li, T. Zhang, S. Tian, C. Li, B. Fu, C. Tang, L. Wang, Z. Li, W. Fan, J. Li, Y. Huang, Z. Liu, Y. Long, C. ang, H. Weng, Y. Shi, H. Lei, Y. Sun, T. Qian, and H. Ding, Observation of unconventional chiral fermions with long Fermi arcs in CoSi, Nature (London) **567**, 496 (2019).

[47] D. Takane, Z. Wang, S. Souma, K. Nakayama, T. Nakamura, H. Oinuma, Y. Nakata, H. Iwasawa, C. Cacho, T. Kim, K. Horiba, H. Kumigashira, T. Takahashi, Y. Ando, and T. Sato, Observation of Chiral Fermions with a Large Topological Charge and Associated Fermi-Arc Surface States in CoSi, Phys. Rev. Lett. **122**, 076402 (2019).

[48] N. B. M. Schröer, D. Pei, M. G. Vergniory, Y. Sun, K. Manna, F. de Juan, J. A. Krieger, V. Süss, M. Schmidt, P. Dudin, B. Bradlyn, T. K. Kim, T. Schmitt, C. Cacho, C. Felser, V. N. Strocov, and Y. Chen, Chiral topological semimetal with multifold band crossings and long Fermi arcs, Nat. Phys. **15**, 759 (2019).

[49] Z. M. Yu, Z. Zhang, G. B. Liu, W. Wu, X. P. Li, R. W. Zhang, S. A. Yang, and Y. Yao, Encyclopedia of emergent particles in three-dimensional crystals, Sci. Bull. **67**, 375 (2022).

[50] A. H. Castro Neto, F. Guinea, N. M. R. Peres, K. S. Novoselov, and A. K. Geim, The electronic properrties of graphene, Rev. Mod. Phys. **81**, 109 (2009).

[51] J. T. Wang, H. Weng, and C. F. Chen, Topological nodal line semimetals in graphene network structures, Adv. Phys. X **4**, 1625724 (2019).

[52] H. Weng, Y. Liang, Q. Xu, R. Yu, Z. Fang, X. Dai, and Y. Kawazoe, Topological node-line semimetal in three-dimensional graphene networks, Phys. Rev. B **92**, 045108 (2015).

[53] J. T. Wang, H. Weng, S. Nie, Z. Fang, Y. Kawazoe, and C. F. Chen, Body-Centered Orthorhombic C_{16}: A Novel Topological Node-Line Semimetal, Phys. Rev. Lett. **116**, 195501 (2016).

[54] Y. Cheng, X. Feng, X. T. Cao, B. Wen, Q. Wang, Y. Kawazoe, and P. Jena, Body-centered tetragonal C_{16}: A novel topological node-line semimetallic carbon composed of tetrarings, Small **13**, 1602894 (2017).

[55] Y. Chen, Y. Xie, S. A. Yang, H. Pan, F. Zhang, M. L. Cohen, and S. B. Zhang, Nanostructured carbon allotropes with Weyl-like loops and points, Nano Lett. **15**, 6974 (2015).

[56] Z. Z. Li, J. Chen, S. Nie, L. F. Xu, H. Mizuseki, H. Weng, and J. T. Wang, Orthorhombic carbon oC24: A novel topological nodal line semimetal, Carbon **133**, 39 (2018).

[57] J. T. Wang, C. F. Chen, and Y. Kawazoe, Topological nodal line semimetal in an orthorhombic graphene network structure, Phys. Rev. B **97**, 245147 (2018).

[58] J. T. Wang, Y. Qian, H. Weng, E. G. Wang, and C. F. Chen, Three-dimensional crystalline modification of graphene in all-sp^2 hexagonal lattices with or without topological nodal lines, J. Phys. Chem. Lett. **10**, 2515 (2019).

[59] Z. Zhao, Y. Hang, Z. Zhang, and W. Guo, Topological hybrid nodal-loop semimetal in a carbon allotrope constructed by interconnected Riemann surfaces, Phys. Rev. B **100**, 115420 (2019).

[60] Z. Zhao, Z. Zhang, and W. Guo, A family of all sp2-bonded carbon allotropes of topological semimetals with strain-robust nodal-lines, J. Mater. Chem. C **8**, 1548 (2020).

[61] J. Liu, X. Li, Q. Wang, Y. Kawazoe, and P. Jena, A new 3D Dirac nodal-line semi-metallic graphene monolith for lithium ion battery anode materials, J. Mater. Chem. A **6**, 13816 (2018).

[62] D. Ni, Y. Shen, W. Sun, and Q. Wang, Design of 3D topological nodal-net porous carbon for sodium-ion battery anodes, J. Mater. Chem. A **10**, 7754 (2022).

[63] Y. Gao, Y. Chen, Y. Xie, P. Y. Chang, M. L. Cohen, and S. Zhang, A class of topological nodal rings and its realization in carbon networks, Phys. Rev. B **97**, 121108(R) (2018).

[64] K. Bu, J. T. Wang, H. Weng, and C. F. Chen, Topological semimetal in an sp^2-sp^3 hybridized carbon network with nodal rings, Phys. Rev. B **101**, 205104 (2020).

[65] K. Bu, Y. Qian, J. T. Wang, and H. Weng, Hybrid nodal chain in an orthorhombic graphene network, Phys. Rev. B **103**, L081108 (2021).

[66] J. T. Wang, S. Nie, H. Weng, Y. Kawazoe, and C. F. Chen, Topological Nodal-Net Semimetal in a Graphene Network Structure, Phys. Rev. Lett. **120**, 026402 (2018).

[67] X. L. Sheng, C. Chen, H. Liu, Z. Chen, Z. M. Yu, Y. X. Zhao, and S. A. Yang, Two-Dimensional Second-Order Topological Insulator in Graphdiyne, Phys. Rev. Lett. **123**, 256402 (2019).

[68] E. Lee, R. Kim, J. Ahn, and B. J. Yang, Two-dimensional higher-order topology in monolayer graphdiyne, npj Quantum Mater. **5**, 1 (2020).

[69] C. Chen, X. T. Zhang, Z. Chen, X. L. Sheng, and S. A. Yang, Second-Order Real Nodal-Line Semimetal in Three-Dimensional Graphdiyne, Phys. Rev. Lett. **128**, 026405 (2022).

[70] H. C. Po, H. Watanabe, and A. Vishwanath, Fragile Topology and Wannier Obstructions, Phys. Rev. Lett. **121**, 126402 (2018).

[71] Z. Song, Z. Wang, W. Shi, G. Li, C. Fang, and B. Andrei Bernevig, All Magic Angles in Twisted Bilayer Graphene are Topological, Phys. Rev. Lett. **123**, 036401 (2019).

[72] Z. Song, B. Lian, N. Regnault, and B. Andrei Bernevig, Twisted bilayer graphene. II. Stable symmetry anomaly Phys. Rev. B **103**, 205412 (2021).

[73] V. Peri, Z. Song, B. Andrei Bernevig, and S. D. Huber, Fragile Topology and Flat-Band Superconductivity in the Strong-Coupling Regime, Phys. Rev. Lett. **126**, 027002 (2021).

[74] J. Herzog-Arbeitman, Z. Song, N. Regnault, and B. Andrei Bernevig, Hofstadter Topology: Noncrystalline Topological Materials at High Flux, Phys. Rev. Lett. **125**, 236804 (2020).

[75] B. Lian, F. Xie, and B. Andrei Bernevig, Landau level of fragile topology, Phys. Rev. B **102**, 041402(R) (2020).

[76] Y. Cao, V. Fatemi, S. Fang, K. Watanabe, T. Taniguchi, E. Kaxiras, and P. J. Herrero, Unconventional superconductivity in magic-angle graphene superlattices, Nature (London) **556**, 43 (2018).

[77] Y. Cao, V. Fatemi, A. Demir, S. Fang, S. L. Tomarken, J. Y. Luo, J. D. S. Yamagishi, K. Watanabe, T. Taniguchi, E. Kaxiras, R. C. Ashoori, and P. J. Herrero, Correlated insulator behaviour at half-filling in magic-angle graphene superlattices, Nature (London) **556**, 80 (2018).

[78] Y. Cao, D. R. Legrain, O. R. Bigorda, J. M. Park, K. Watanabe, T. Taniguchi, and P. J. Herrero, Tunable correlated states and spin-polarized phases in twisted bilayer–bilayer graphene, Nature (London) **583**, 215 (2020).

[79] Y. Cao, J. M. Park, K. Watanabe, T. Taniguchi, and P. J. Herrero, Pauli-limit violation and re-entrant superconductivity in moiré graphene, Nature (London) **595**, 526 (2021).

[80] R. Hoffmann, T. Hughbanks, M. Kertesz, and P. H. Bird, Hypothetical metallic allotrope of carbon, J. Am. Chem. Soc. **105**, 4831 (1983).

[81] Y. Zhou, K. H. Jin, H. Huang, Z. Wang, and F. Liu, Weyl points created by a three-dimensional flat band, Phys. Rev. B **99**, 201105(R) (2019).

[82] G. Sethi, Y. Zhou, L. Zhu, L. Yang, and F. Liu, Flat-Band-Enabled Triplet Excitonic Insulator in a Diatomic Kagome Lattice, Phys. Rev. Lett. **126**, 196403 (2021).

[83] R. K. Choudhary, S. C. Mishra, P. Mishra, P. K. Limaye, and P. U. Sastry, Mechanical and tribological properties of rhombohedral diamond-rich coatings grown on stainless steel by hot filament CVD, Trans. IMF **95**, 197 (2017).

[84] G. Kresse and J. Furthüller, Effcient iterative schemes for *ab initio* total-energy calculations using a plane-wave basis set, Phys. Rev. B **54**, 11169 (1996).

[85] R. Armiento and A. E. Mattsson, Functional designed to include surface effects in self-consistent density functional theory, Phys. Rev. B **72**, 085108 (2005).

[86] P. E. Blöchl, Projector augmented-wave method, Phys. Rev. B **50**, 17953 (1994).

[87] J. P. Perdew, K. Burke, and M. Ernzerhof, Generalized Gradient Approximation Made Simple, Phys. Rev. Lett. **77**, 3865 (1996).

[88] J. Heyd, G. E. Scuseria, and M. Ernzerhof, Hybrid functionals based on a screened Coulomb potential, J. Chem. Phys. **118**, 8207 (2003).

[89] A. Togo, F. Oba, and I. Tanaka, First-principles calculations of the ferroelastic transition between rutile-type and $CaCl_2$-type SiO_2 at high pressures, Phys. Rev. B **78**, 134106 (2008).

[90] A. A. Mostofi, J. R. Yates, Y. S. Lee, I. Souza, D. Vanderbilt, and N. Marzari, Wannier90: A tool for obtaining maximally-localised Wannier functions, Comput. Phys. Commun. **178**, 685 (2008).

[91] N. Marzari, A. A. Mostofi, J. R. Yates, I. Souza, and D. Vanderbilt, Maximally localized Wannier functions: Theory and applications, Rev. Mod. Phys. **84**, 1419 (2012).

[92] Q. S. Wu, S. N. Zhang, H. F. Song, M. Troyer, and A. A. Soluyanov, WannierTools : An open-source software package for novel topological materials, Comput. Phys. Commun. **224**, 405 (2018).

[93] F. D. Murnaghan, The compressibility of media under extreme pressures, Proc. Natl. Acad. Sci. USA **30**, 244 (1944).

[94] F. Occelli, P. Loubeyre, and R. LeToullec, Properties of diamond under hydrostatic pressures up to 140 GPa, Nat. Mater. **2**, 151 (2003).

[95] Z. J. Wu, E. J. Zhao, H. P. Xiang, X. F. Hao, X. J. Liu, and J. Meng, Crystal structures and elastic properties of superhard IrN_2 and $IrN_3$3 from first principles, Phys. Rev. B **76**, 054115 (2007).

[96] S. Nosé, A unified formulation of the constant temperature molecular dynamics methods, J. Chem. Phys. **81**, 511 (1984).

[97] See Supplemental Material at http://link.aps.org/supplemental/10.1103/PhysRevB.107.245111 for: (1) *ab initio* molecular dynamics simulations at 300 and 600 K; (2) Partial density of states, fat band analysis, and Wannier tight-binding model; (3) Parities at the time reversal invariant momenta. This includes Refs. [90,91,96].

[98] S. Ryu and Y. Hatsugai, Topological Origin of Zero-Energy Edge States in Particle-Hole Symmetric Systems, Phys. Rev. Lett. **89**, 077002 (2002).

[99] G. Bian, T. R. Chang, R. Sankar, S.-Y. Xu, H. Zheng, T. Neupert, C.-K. Chiu, S.-M. Huang, G. Chang, I. Belopolski, D. S. Sanchez, M. Neupane, N. Alidoust, C. Liu, B. Wang, H.-T. Jeng, A. Bansil, F. Chou, H. Lin, and M. Z. Hasan, Topological nodal-line fermions in spin-orbit metal $PbTaSe_2$, Nat. Commun. **7**, 10556 (2016).